

Article

Optimal Scheduling of Residential Microgrids Considering Virtual Energy Storage System

Weiliang Liu *, Changliang Liu, Yongjun Lin, Liangyu Ma, Kang Bai and Yanqun Wu

State Key Laboratory of Alternate Electrical Power System with Renewable Energy Sources, North China Electric Power University, Baoding 071003, China; 13603123513@163.com (C.L.); lin3172@126.com (Y.L.); maliangyu@ncepu.edu.cn (L.M.); pisa_kang@126.com (K.B.); 15720123548@163.com (Y.W.)

* Correspondence: lwlwfengzhiying@163.com; Tel.: +86-159-3357-9831

Received: 1 March 2018; Accepted: 10 April 2018; Published: 16 April 2018



Abstract: The increasingly complex residential microgrids (r-microgrid) consisting of renewable generation, energy storage systems, and residential buildings require a more intelligent scheduling method. Firstly, aiming at the radiant floor heating/cooling system widely utilized in residential buildings, the mathematical relationship between the operative temperature and heating/cooling demand is established based on the equivalent thermodynamic parameters (ETP) model, by which the thermal storage capacity is analyzed. Secondly, the radiant floor heating/cooling system is treated as virtual energy storage system (VESS), and an optimization model based on mixed-integer nonlinear programming (MINLP) for r-microgrid scheduling is established which takes thermal comfort level and economy as the optimization objectives. Finally, the optimal scheduling results of two typical r-microgrids are analyzed. Case studies demonstrate that the proposed scheduling method can effectively employ the thermal storage capacity of radiant floor heating/cooling system, thus lowering the operating cost of the r-microgrid effectively while ensuring the thermal comfort level of users.

Keywords: microgrid; residential buildings; optimal scheduling; radiant floor heating/cooling; virtual energy storage; operative temperature; operating cost

1. Introduction

Recently, with the growing concerns over the energy depletion and environmental issues around the world, technologies in renewable generation utilization and energy efficiency improvement have attracted increasing attention [1]. According to a report from the International Energy Agency, energy consumption of buildings occupies about 32% of the global energy consumption and they are responsible for approximately 30% of total end-use and energy-related CO₂ emissions [2]. In China, energy consumption of buildings currently accounts for 27.6% of the total energy consumption and it is estimated to reach 35% by 2020 [3,4]. Therefore, specific initiatives are needed to encourage a high penetration of renewable generation and low energy consumption for buildings.

Microgrid technology presents a good opportunity and a desirable infrastructure for enhancing the efficiency of energy utilization of buildings. However, there are many challenges that need to be addressed. For example, the operation of different types of energy supplies like renewable generation, dispatchable distribution generators (DGs), and energy storage systems are coupled and need to be well coordinated. In addition, energy balance as well as complicated operating constraints of energy supplies should be satisfied at the same time. Therefore, an intelligent scheduling method for building microgrids is required and is a current research hotspot.

Various studies have been carried out for scheduling microgrids. Guan et al. [5] developed an economic scheduling model for a low-carbon building to minimize the total cost of natural gas

and electricity. Xu et al. [6] proposed hierarchical energy management system for the multisource multi-product microgrids based on an energy hub model. Jaramillo et al. [7] proposed a multi-objective mixed-integer linear programming (MILP) model to reduce the daily operating cost and the total emission of a hybrid energy microgrid. Lu et al. [8] proposed a mixed-integer nonlinear programming (MINLP) model to solve the economic scheduling for a building microgrid and deal with the discrete working scopes of the energy systems. Zhao et al. [9] developed a strategy based on predictive control model and nonlinear programming was used to schedule a building microgrid under dynamic electricity prices. Li et al. [10] proposed a combined heat and power scheduling model for regional grid-connected microgrids to obtain the optimal costs and operation modes of the microsources. Wu et al. [11] proposed a MILP model to realize the economic scheduling of a microgrid.

Energy storage systems (ESS) play a crucial part in the optimal scheduling of microgrids. Electric energy storage systems—i.e., storage batteries or super capacitors—have the advantages of high energy density and rapid response speed, while being quite expensive for large-capacity configuration. Thermal energy storage systems—i.e., heat storage tanks or cool storage tanks—have the advantage of lower construction cost, however, they are often limited in practical applications due to higher space requirements. Recently, novel ways to enhance the energy efficiency and economy of microgrids by scheduling the demand side controllable load—like water heaters, air conditioners, freezers, heat pumps, refrigerators, electric vehicles (EVs), etc.—of which the normal power consumption patterns can be changed have come to the fore. Lu et al. [12] studied the potential of providing load smoothing service of direct load control of HVAC system. On this basis, Wang et al. [13] took the state sequence control of electric heat pump as an example, constructed a generalized energy storage system to smooth the fluctuation of tie-line power for microgrids. Ai et al. [14] studied virtual energy storage characteristics of air conditioning load and dissipated wind power fluctuations based on direct load control. Jia et al. [15] took the refrigerator as an example, proposed the control strategy of family-friendly loads to realize the frequency response of autonomous microgrids. Jin et al. [16,17] built a virtual energy storage system (VESS) considering heat capacity of indoor air and insulation characteristics of buildings, and proposed a scheduling method for hybrid energy microgrid to minimize daily operating costs and ensure thermal comfort level. Van et al. [18] discussed the charging strategy of the EVs for an office building microgrid including a photovoltaic (PV) system, and a combined heat and power unit. Igualada et al. [19] proposed an economic dispatch model for a residential microgrid consisting of renewable energy sources and a vehicle-to-grid system to reduce the daily operating cost. Rabiee et al. [20] proposed a multi-objective dispatch model for a microgrid containing EVs, responsive loads, and renewable generation to lower the total emissions and the daily operating costs.

At present, radiant floor heating systems have been widely utilized in residential buildings, while the corresponding cooling systems are gradually maturing [21,22]. Owing to the considerable thermal storage capacity of the radiant floor and envelope structure, it is quite promising to treat the radiant floor heating/cooling system as a demand side controllable load and introduce it into the optimal scheduling of residential microgrids. However, to the authors' best knowledge, few studies have been carried out about this point. Therefore, the major objective of this paper is to present a novel r-microgrid scheduling method with VESS based on radiant floor heating/cooling system. Firstly, the mathematical model of radiant floor heating/cooling system is established based on the equivalent thermodynamic parameters (ETP) model, by which the thermal storage capacity is analyzed. Secondly, treating radiant floor heating/cooling systems as VESSs, an optimization model based on MINLP for r-microgrid scheduling is established which takes thermal comfort level and economy as the optimization objectives. Finally, the optimal scheduling results of two typical r-microgrids are analyzed. Accordingly, the contents in this paper comprise the following five parts: typical structure of r-microgrids (Section 1); energy storage characteristics of radiant floor heating/cooling systems (Section 2); an optimization model for r-microgrid scheduling with VESS (Section 3); a case study (Section 4); the conclusion (Section 5).

2. Typical Structure of R-Microgrids

2.1. Typical Structure of R-Microgrids

In this paper, two kinds of typical r-microgrids are studied, of which the network architectures are similar with that of the smart grid referenced in the literature [23]. The first one is the electric heating/cooling microgrid, the structure of which is shown in Figure 1a. It is connected to an external grid allowing electric power exchange, and integrated with renewable generations—i.e., wind generation (WT) and photovoltaic generation (PV)—and a battery energy storage system (BESS) [24], and other devices—i.e., electric heaters (EHs) and electric chillers (ECs)—to satisfy the electric load and heating/cooling demand of the residential buildings. The second one is the Combined Cooling Heating and Power (CCHP) microgrid, the structure of which is shown in Figure 1b. Compared with the electric heating/cooling microgrid, a CCHP unit consisting of micro-gas turbines (MTs), a waste heat recovery system, and absorption chillers (ACs) is introduced in to satisfy the heating/cooling demand instead of EHs and ECs, which operates with the strategy of following the thermal load (FTL), in other words, the output electric power is fully determined by the output thermal power.

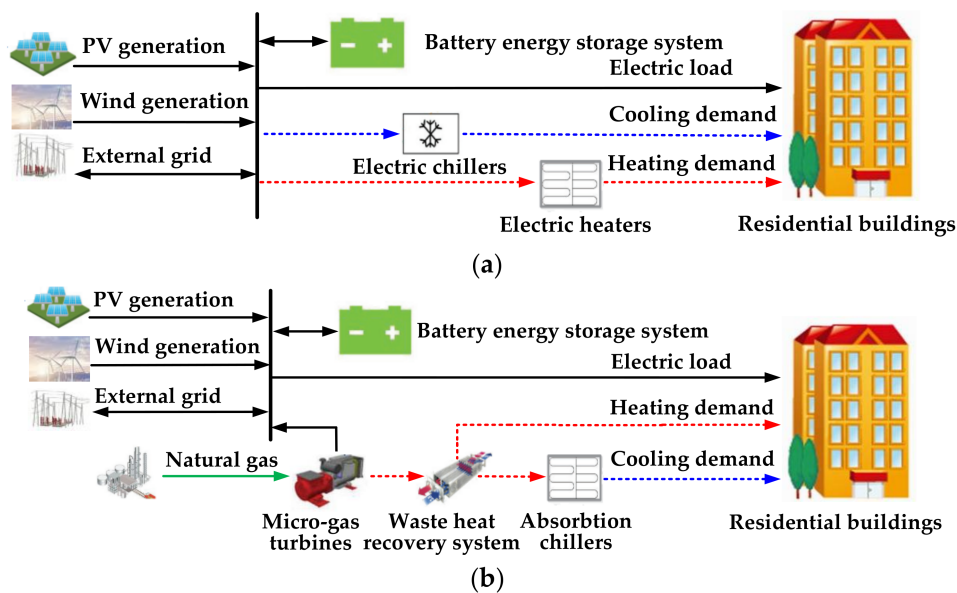


Figure 1. Structure of typical r-microgrids studied in this paper. (a) Electric heating/cooling microgrid; (b) CCHP microgrid.

2.2. Equipment Principal

(1) CCHP Unit

MTs generate electricity by consuming natural gas, and the output electric power P_{MT} is

$$P_{MT} = F_{gas} \times L_{HVNG} \times \eta_{MT} \quad (1)$$

at the same time, the output thermal power Q_{MT} is

$$Q_{MT} = P_{MT} \times \frac{1 - \eta_{MT} - \eta_L}{\eta_{MT}} \quad (2)$$

where F_{gas} is the natural gas consumed per unit time by MTs, L_{HVNG} is the low calorific value of natural gas, η_{MT} and η_L are the power generation efficiency and heat loss rate of the MTs respectively.

The output thermal power Q_{MT} can be converted to the heating power Q_{MTH} through the waste heat recovery system

$$Q_{MTH} = Q_{MT} \times \eta_{HE} \quad (3)$$

where η_{HE} is the efficiency of waste heat recovery system, or can be further converted to the cooling power Q_{MTC} through the ACs

$$Q_{MTC} = Q_{MT} \times \eta_{HE} \times COP_{AC} \quad (4)$$

where COP_{AC} is the coefficient of performance (COP) of the ACs.

(2) Electric Heaters/Chillers

The EHs generate heat by consuming electric energy, and the heating power Q_{EH} is

$$Q_{EH} = P_{EH} \times COP_{EH} \quad (5)$$

where P_{EH} and COP_{EH} are the consumed electric power and COP of the EHs respectively. Similarly, the ECs generate cool by consuming electric energy, and the cooling power Q_{EC} is

$$Q_{EC} = P_{EC} \times COP_{EC} \quad (6)$$

where P_{EC} and COP_{EC} are the consumed electric power and COP of the ECs respectively.

(3) Battery Energy Storage System

During the scheduling process, the state of charge (SOC) of the BESS changes according to the formula

$$E^t = E^{t-1} + \Delta T \times U_{Si+}^t \times P_{Si+}^t \times \eta_c - \Delta T \times U_{Si-}^t \times \frac{P_{Si-}^t}{\eta_{disc}} \quad (7)$$

where E^t and E^{t-1} are the SOCs of the BESS at the end of scheduling period $t - 1$ and t respectively, P_{Si+}^t / P_{Si-}^t is the charging/discharging power of BESS during scheduling period t , U_{Si+}^t / U_{Si-}^t is the charging/discharging status of scheduling period t , η_c / η_{disc} is the charging/discharging efficiency, and ΔT is the duration of scheduling period t .

3. Energy Storage Characteristics of Radiant Floor Heating/Cooling Systems

3.1. Model of Radiant Floor Heating/Cooling Systems

Depending on the structure and materials, radiant floors could be classified into heavy floors and light floors [22]. Different with traditional air conditioning heating/cooling systems that transfer heat to the human body mainly by indoor air convection, the radiant floor heating/cooling system transfers heat to human body mainly by thermal radiation of floor and envelope structure (walls and windows). Thus, the operative temperature, which is the mean value of indoor average radiation temperature and air temperature, is suited for evaluating the thermal comfort level [25]. The influencing factors of operative temperature mainly include heating/cooling demand, solar radiation load, and heat/cold dissipation caused by the difference between indoor and outdoor temperatures. Based on the work of [12], in this paper, the mathematical relationship between the operative temperature and heating/cooling demand is established based on the equivalent thermodynamic parameters (ETP) model, as shown in Figure 2.

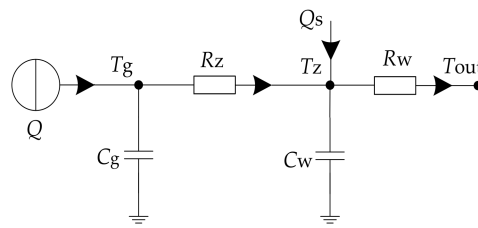


Figure 2. Equivalent thermodynamic parameters (ETP) model for radiant floor heating/cooling system.

In Figure 2, Q is the heating/cooling demand (W), Q_s is the solar radiation load (W), T_g is the radiant floor surface temperature ($^{\circ}\text{C}$), T_z is the operative temperature ($^{\circ}\text{C}$), T_{out} is the outdoor temperature ($^{\circ}\text{C}$), C_g is the equivalent heat capacity of the radiant floor ($\text{J}/^{\circ}\text{C}$), C_w is the equivalent heat capacity ($\text{J}/^{\circ}\text{C}$) of the envelope structure, R_z is the equivalent heat resistance of convection and radiation between the radiant floor surface and the indoor air as well as the envelope structure ($^{\circ}\text{C}/\text{W}$), and R_w is the equivalent thermal resistance of the envelope structure ($^{\circ}\text{C}/\text{W}$).

The differential equations for thermal power balance corresponding to the above ETP model are

$$C_g \frac{dT_g}{dt} = Q - \frac{T_g - T_z}{R_z} \quad (8)$$

$$C_w \frac{dT_z}{dt} = \frac{T_g - T_z}{R_z} + Q_s - \frac{(T_z - T_{\text{out}})}{R_w} \quad (9)$$

Considering the specific structure of residential buildings and the thermal physical parameters of materials, Equations (8) and (9) can be expressed as

$$A_g \times C_{g1} \frac{dT_g}{dt} = Q - A_g \times h_z (T_g - T_z) \quad (10)$$

$$(A_{wi} \times C_{wi} + A_{wa} \times C_{wa}) \frac{dT_z}{dt} = A_g h_z (T_g - T_z) + A_{wi} \times I \times \alpha - (A_{wi} k_{wi} + A_{wa} k_{wa}) (T_z - T_{\text{out}}) \quad (11)$$

where A_g , A_{wa} , and A_{wi} are respectively the total area of radiant floor, external wall, and external window in residential building (m^2); C_{g1} , C_{wa} , and C_{wi} are respectively the equivalent heat capacity of radiant floor, external wall, and external window ($\text{kJ}/(\text{m}^2 \cdot ^{\circ}\text{C})$); h_z is the comprehensive heat transfer coefficient of radiation and convection from the radiant floor surface to the indoor air and the envelope structure ($\text{W}/\text{m}^2 \cdot ^{\circ}\text{C}$); k_{wi} and k_{wa} are the heat transfer coefficient of the external wall and the external window of the envelope structure respectively; I is the solar radiation intensity; α is the shading coefficient, the value of which is related to the glass material of window and whether there is a sun visor or not.

3.2. Energy Storage Characteristics of Radiant Floor Heating/Cooling Systems

In order to analyze the energy storage characteristics of radiant floor heating/cooling systems, taking the heating in winter as example, the influence of heating demand disturbance on operative temperature is simulated using the established ETP model. A residential building with 100 households is chosen as an example, which is 30 m long, 20 m wide, and 70 m high. The total areas of the radiation floor and envelope structure (window to wall ratio is 0.3, shading coefficient α is 0.2) are $10,600 \text{ m}^2$ and 7100 m^2 respectively. Thermal physical parameters of the radiant floor and the envelope structure are shown in Tables 1 and 2, respectively.

Table 1. Structure and thermal physical parameters of radiant floor system [22].

Type	Layers and Materials	Comprehensive Heat Transfer Coefficient (W/(m ² ·°C))	Equivalent Heat Capacity (kJ/(m ² ·°C))
Heavy floor	25 mm marble + 25 mm cement mortar + 70 mm concrete (embedded diameter 20 mm pipe, spacing 150 mm)	11	148.1
Light floor	5 mm marble + 0.3 mm aluminum foil + 20 mm coagulating (embedded diameter 20 mm pipe, spacing 150 mm)	11	17.4

Table 2. Thermal physical parameters of envelope structure [16].

Type	Materials	Heat Transfer Coefficient (W/(m ² ·°C))	Equivalent Heat Capacity (kJ/(m ² ·°C))
External window	Ordinary hollow glass + PV plastic window	2.80	6.0
External wall	25 mm cement mortar + 190 mm single row hole block + 25 mm adiabatic mortar	1.50	62

(1) Simulation Process One

The simulation process one assumes that the solar radiation load $Q_s = 0$, and the outdoor temperature is $T_{out} = -8$ °C. At the moment $t = 0$ h, the radiant floor heating system works in a steady state: $T_z = 22$ °C, $T_g = 25.5$ °C, $Q = 379$ kW, and heating demand disturbance $\Delta Q = -100$ kW, -200 kW, -379 kW is implemented respectively at the moment $t = 10$ h, the changing processes of T_z and T_g are shown in Figure 3. It can be seen that T_z and T_g begin to decrease slowly when heating demand disturbance is implemented, and it takes quite a long time to achieve the new steady state. For light radiant floor heating systems, the required times for T_z decreasing from 22 °C to 17 °C are 11.4 h, 4.6 h, and 2.4 h respectively corresponding to $\Delta Q = -100$ kW, -200 kW, -379 kW; while for heavy radiant floor heating systems, the above required times become dramatically longer, 45.1 h, 17.4 h, and 8.6 h respectively.

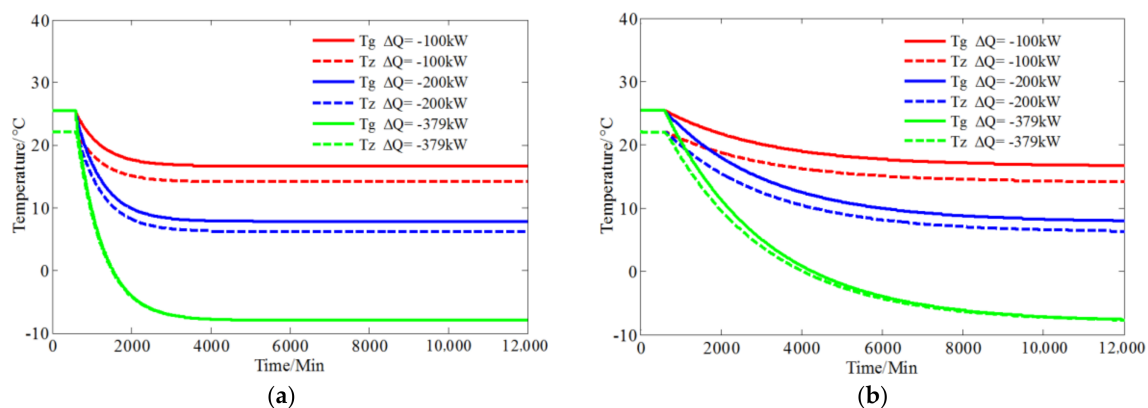


Figure 3. Simulation process one for radiant floor heating system. (a) Light radiant floor heating system; (b) heavy radiant floor heating system.

(2) Simulation Process Two

Assumes the simulation process two has the same initial conditions as the simulation process one, and heating demand disturbances $\Delta Q = 100$ kW, 200 kW, and 379 kW are implemented respectively at $t = 10$ h, the changing process of T_z and T_g are shown in Figure 4. It can be seen that T_z and T_g begin to rise slowly when heating demand disturbance is implemented, and it takes quite a long time to achieve the new steady state. For light radiant floor heating systems, the required times for T_z rising from 22 °C to 27 °C are 10.6 h, 4.5 h, and 2.3 h respectively corresponding to $\Delta Q = 100$ kW, 200 kW, and 379 kW; while for heavy radiant floor heating systems, the above required times also become dramatically longer at 41.6 h, 16.3 h, and 8.2 h respectively.

Through above simulation processes, it is known that the operative temperature changes quite slowly when heating demand disturbance is implemented owing to the considerable thermal storage capacity of the radiant floor and envelope structure. Based on this characteristic, the radiant floor heating/cooling system is treated as a virtual energy storage system (VESS) here, and is integrated into the optimization model for r-microgrid scheduling, then the heating/cooling demand could be scheduled to fully tap the energy storage potential of the VESS while ensuring the thermal comfort level of the user.

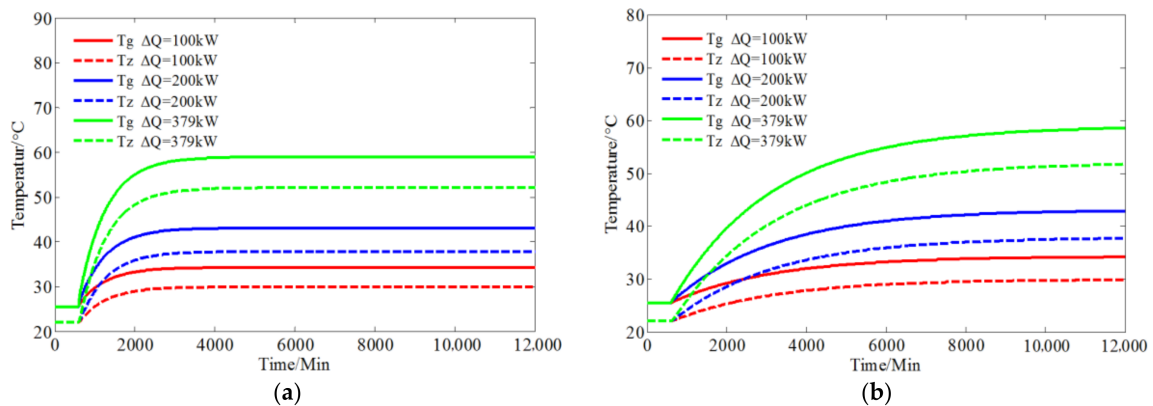


Figure 4. Simulation process two for radiant floor heating system. (a) Light floor radiant heating system; (b) heavy floor radiant heating system.

4. Optimization Model for R-Microgrid Scheduling

4.1. Parameters to Be Optimized

This paper takes heating in winter as well as cooling in summer as examples to establish the MINLP optimization model of for r-microgrid scheduling. The variables that need to be optimized include control variables and state variables of all scheduling periods θ_T . For scheduling period t , the control variables are shown in Table 3, and the state variables are shown in Table 4.

Table 3. Control variables for scheduling period t .

Variables	Variable Description
U_{MT}^t	Operation status of MTs, 1—'ON' state, 0—'OFF' state
P_{MT}^t	Output electric power of MTs
U_{Si+}^t	Charging status of BESS, 1—charging state, 0—non charging state
U_{Si-}^t	Discharging status of BESS, 1—discharging state, 0—non discharging state
P_{Si+}^t	Charging power of BESS
P_{Si-}^t	Discharging power of BESS
U_{grid+}^t	Status for purchasing power from external grid, 1—purchasing, 0—non purchasing
U_{grid-}^t	Status for selling power to external grid, 1—selling, 0—non selling
P_{grid+}^t	Power purchasing from external grid
P_{grid-}^t	Power Selling to external grid
U_{EH}^t	Operation status for EHs, 1—'ON' state, 0—'OFF' state
U_{EC}^t	Operation status for ECs, 1—'ON' state, 0—'OFF' state
P_{EH}^t	Electric power consumed by EHs
P_{EC}^t	Electric power consumed by ECs

Table 4. State variables for scheduling period t .

Variables	Variable Description
Q_{MT}^t	Output thermal power of MTs
η_{MT}^t	Power generation efficiency of MTs
E^t	SOC of BESS
T_g^t	Radiant floor surface temperature
T_z^t	Operative temperature

4.2. Objective Function

The objective function of the optimization model includes two parts: thermal comfort level objective function and economy objective function.

4.2.1. Thermal Comfort Level Objective Function

Thermal comfort represents the peoples' subjective perception to the thermal environment. In order to reflect the hot and cold feeling of the vast majority of people to the same thermal environment, [26] proposed the predicted mean vote (PMV), which divides the thermal sensation into seven scales, as shown in Table 5. PMV can be calculated by six parameters: air temperature t_a , average radiation temperature t_r , air velocity v_{ar} , relative humidity h , human metabolic rate M , and clothing thermal resistance I_{cl} .

Table 5. Thermal sense scale of predicted mean vote (PMV).

Thermal Sense	Cold	Cool	Slightly Cool	Well Suitable	Slightly Warm	Warm Hot
Value of PMV	−3	−2	−1	0	1	2 3

Considering further the differences among individuals in physiology, psychology, and behavioral characteristics, ref. [26] also proposed the predicted percentage of dissatisfied (PPD) to indicate the

peoples' dissatisfaction with the thermal environment. The relationship between PPD and PMV can be calculated as

$$PPD = 100 - 95e^{-(0.03353 \times PMV^4 + 0.2179 \times PMV^2)} \quad (12)$$

According to the national standards of the PRC "Moderate thermal environments—Determination of the PMV and PPD indices and specification of the conditions for thermal comfort" (GB/T 18049-2000), the value of PMV and PPD should be: $-1 \leq PMV \leq +1$, $PPD \leq 27\%$. Considering the peoples' habits and dressing characteristics in residential buildings, this paper takes $M = 69.78 \text{ W/m}^2$, $v_{ar} = 0.1 \text{ m/s}$, $h = 50\%$ for winter and summer, and $I_{cl} = 1 \text{ m}^2 \cdot ^\circ\text{C/W}$ for winter while $I_{cl} = 0.5 \text{ m}^2 \cdot ^\circ\text{C/W}$ for summer, and ignores the difference between the average radiation temperature t_r and the air temperature t_a , that is, $t_a = t_r = T_z$, then calculates the values of PMV and PPD under different operative temperature T_z , as shown in Figure 5.

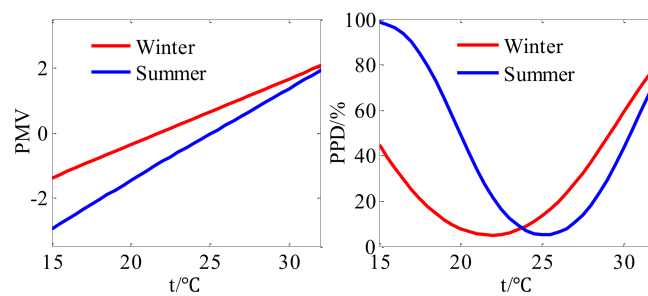


Figure 5. Values of PMV and PPD under different operative temperature T_z .

It is known from Figure 5 that corresponding to $PMV = 0$, the optimum operative temperature T_{zopt} is $22 \text{ }^\circ\text{C}$ for winter, and $25 \text{ }^\circ\text{C}$ for summer. While corresponding to $-1 \leq PMV \leq +1$, $PPD \leq 27\%$, the variation range of T_z is $17 \sim 27 \text{ }^\circ\text{C}$ for winter, and is $21.5 \sim 29 \text{ }^\circ\text{C}$ for summer, which makes it is quite possible to schedule the heating/cooling demand.

In order to ensure a higher thermal comfort level, in this paper, the permitted adjustable range of T_z is $\pm 2.5 \text{ }^\circ\text{C}$ during the scheduling of heating/cooling demand, and thermal comfort level objective function is calculated as the quadratic sum of deviations of actual operative temperature and optimum operative temperature for all scheduling periods

$$\min f_1(x_s) = \sum_{t \in \theta_T} |T_z^t - T_{zopt}|^2 \quad (13)$$

4.2.2. Economy Objective Function

The operating cost of the r-microgrid includes: cost for natural gas, cost for charging/discharging of BESS, cost for power exchange with external grid, and maintenance cost of renewable generation and devices. The economy objective function is constructed as

$$\min f_2(x_s) = f_G(x_s) + f_S(x_s) + f_{Grid}(x_s) + f_{RMC}(x_s) \quad (14)$$

In Formula (14), f_G is the cost for natural gas

$$f_G(x_s) = \sum_{t \in \theta_T} c_{gas} F_{gas}^t \quad (15)$$

where c_{gas} is price of natural gas, F_{gas}^t is the natural gas consumed by MTs at scheduling period t .

f_S is the cost for charging/discharging of BESS

$$f_S(x_s) = \sum_{t \in \theta_T} (c_{Si+} U_{Si+}^t P_{Si+}^t + c_{Si-} U_{Si-}^t P_{Si-}^t) \Delta T \quad (16)$$

where c_{Si+} is the unit cost for charging and c_{Si-} is the unit cost for discharging.

f_{Grid} is the cost for power exchange with external grid

$$f_{Grid}(x_s) = \sum_{t \in \theta_T} (c_{grid+}^t U_{grid+}^t P_{grid+}^t - c_{grid-}^t U_{grid-}^t P_{grid-}^t) \Delta T \quad (17)$$

where c_{grid+}^t is the price for purchasing electricity from external grid at scheduling period t , c_{grid-}^t is the price for selling electricity to external grid at scheduling period t .

f_{RMC} is the maintenance cost of renewable generation and devices in r-microgrids

$$f_{RMC}(x_s) = \sum_{t \in \theta_T} (c_{PV} P_{PV}^t + c_{WT} P_{WT}^t + c_{EH} P_{EH}^t U_{EH}^t + c_{EC} P_{EC}^t U_{EC}^t + c_{MT} P_{MT}^t U_{MT}^t + c_{AC} Q_{AC}^t U_{MT}^t) \Delta T \quad (18)$$

where P_{PV}^t and P_{WT}^t are the output power of PV and WT respectively at scheduling period t , c_{PV} , c_{WT} , c_{EH} , c_{EC} , c_{MT} , and c_{AC} are the unit maintenance costs of PV, WT, EHs, ECs, MTs, and ACs respectively.

Considering the thermal comfort level objective function is conflict with the economy objective function, thermal comfort sensitive coefficient is introduced in to balance them, then the total objective function of the optimization model for r-microgrid scheduling is constructed as

$$\min f(x_s) = \gamma \cdot f_1(x_s) + f_2(x_s) \quad (19)$$

where γ is the thermal comfort sensitive coefficient, which could be regarded as the penalty coefficient for the decline of thermal comfort level.

4.3. Constraint Conditions

(1) Constraint for electric power balance

$$P_{load}^t + U_{EH}^t P_{EH}^t + U_{EC}^t P_{EC}^t = P_{PV}^t + P_{WT}^t + U_{MT}^t P_{MT}^t - U_{Si+}^t P_{Si+}^t + U_{Si-}^t P_{Si-}^t + U_{grid+}^t P_{grid+}^t - U_{grid-}^t P_{grid-}^t, \forall t \in \theta_T \quad (20)$$

where P_{load}^t is the forecasted electric load (except for the electric power consumed by EHs and ECs) at scheduling period t .

(2) Constraints for thermal power balance

The heat dissipation and operative temperature changing of residential buildings is a slow dynamic process. Therefore, in order to solve the optimization model conveniently, differential Equations (10) and (11) are converted to difference equations to express the constraint of thermal power balance for residential buildings

$$T_g^{t+1} = T_g^t + \frac{\Delta T}{A_g C_{g1}} \times [Q^t - A_g h_z (T_g^t - T_z^t)], \forall t \in \theta_T \quad (21)$$

$$T_z^{t+1} = T_z^t + \frac{\Delta T}{(A_{wi} C_{wi} + A_{wa} C_{wa})} \times [A_g h_z (T_g^t - T_z^t) + A_{wi} \times I^t \times \alpha - (A_{wi} k_{wi} + A_{wa} k_{wa}) (T_z^t - T_{out}^t)], \forall t \in \theta_T \quad (22)$$

where for heating in winter, there is

$$Q^t = U_{MT}^t Q_{MT}^t \eta_{HE} + U_{EH}^t P_{EH}^t COP_{EH}, \forall t \in \theta_T \quad (23)$$

While for cooling in summer, there is

$$Q^t = -U_{MT}^t Q_{MT}^t \eta_{HE} COP_{AC} - U_{EC}^t P_{EC}^t COP_{EC}, \forall t \in \theta_T \quad (24)$$

(3) Constraints for battery energy storage system

For BESS, constraint for state uniqueness is

$$U_{Si+}^t + U_{Si-}^t \leq 1, \forall t \in \theta_T \quad (25)$$

The charging/discharging power and the SOC should meet the upper and lower limits

$$\underline{P}_{Si+} \leq P_{Si+}^t \leq \overline{P}_{Si+}, \forall t \in \theta_T \quad (26)$$

$$\underline{P}_{Si-} \leq P_{Si-}^t \leq \overline{P}_{Si-}, \forall t \in \theta_T \quad (27)$$

$$\underline{E} \leq E^t \leq \overline{E}, \forall t \in \theta_T \quad (28)$$

where \overline{P}_{Si+} and \underline{P}_{Si+} are respectively the upper and lower limits for charging power, \overline{P}_{Si-} and \underline{P}_{Si-} are respectively the upper and lower limits for discharging power, \overline{E} and \underline{E} are respectively the upper and lower limits for SOC.

At the end of scheduling process, the SOC should be same as the initial SOC for energy balance

$$E^0 = E^N \quad (29)$$

(4) Constraints for power exchange with external grid

For power exchange with external grid, constraint for state uniqueness is

$$U_{grid+}^t + U_{grid-}^t \leq 1, \forall t \in \theta_T \quad (30)$$

The power exchange should meet the upper and lower limits

$$\underline{P}_{grid+} \leq P_{grid+}^t \leq \overline{P}_{grid+}, \forall t \in \theta_T \quad (31)$$

$$\underline{P}_{grid-} \leq P_{grid-}^t \leq \overline{P}_{grid-}, \forall t \in \theta_T \quad (32)$$

where \overline{P}_{grid+} and \underline{P}_{grid+} are respectively the upper and lower limits for power purchasing from external grid, \overline{P}_{grid-} and \underline{P}_{grid-} are respectively the upper and lower limits for selling power to the external grid.

(5) Constraints for MTs

The output electric power of MTs should meet the lower and upper limits

$$\underline{P}_{MT} \leq P_{MT}^t \leq \overline{P}_{MT}, \forall t \in \theta_T \quad (33)$$

where \overline{P}_{MT} and \underline{P}_{MT} are respectively the upper and lower limits of the output electric power of MTs.

Generally, there is a nonlinear relationship between η_{MT} and P_{MT} , this paper uses the fourth-order polynomial to fit this relationship in order to facilitate the subsequent calculation. Take Capstone's C200 type MT as example, the polynomial equation obtained is

$$\eta_{MT}^t = \alpha_1 \left(\frac{P_{MT}^t}{P_{MT}^{\max}} \right)^4 + \alpha_2 \left(\frac{P_{MT}^t}{P_{MT}^{\max}} \right)^3 + \alpha_3 \left(\frac{P_{MT}^t}{P_{MT}^{\max}} \right)^2 + \alpha_4 \left(\frac{P_{MT}^t}{P_{MT}^{\max}} \right) + \alpha_5, \forall t \in \theta_T \quad (34)$$

where $\alpha_1 = -65.808$, $\alpha_2 = -183.36$, $\alpha_3 = -203.76$, $\alpha_4 = 111.74$, $\alpha_5 = 7.019$, and P_{MT}^{\max} is the rated power of the MT.

(6) Constraints for EHs and ECs

Electric power consumed by EHs and ECs should meet the lower and upper limits

$$\underline{P}_{EH} \leq P_{EH}^t \leq \overline{P}_{EH}, \forall t \in \theta_T \quad (35)$$

$$\underline{P}_{EC} \leq P_{EC}^t \leq \overline{P}_{EC}, \forall t \in \theta_T \quad (36)$$

where \overline{P}_{EH} and \underline{P}_{EH} are respectively the upper and lower limits of the electric power consumed by EHs, \overline{P}_{EC} and \underline{P}_{EC} are respectively the upper and lower limits of the electric power consumed by ECs.

(7) Constraints for operative temperature

$$\underline{T}_z \leq T_z^t \leq \overline{T}_z, \forall t \in \theta_T \quad (37)$$

where \overline{T}_z and \underline{T}_z are respectively the upper and lower limits of operative temperature.

At the end of scheduling process, the operative temperature should be same as the initial operative temperature to ensure the balance of total energy stored in the residential building

$$T_z^0 = T_z^N \quad (38)$$

For cooling in summer, in order to prevent condensation phenomenon, the radiant floor surface temperature should be higher than the dew-point temperature

$$T_g^t > \underline{T}_g, \forall t \in \theta_T \quad (39)$$

where \underline{T}_g is the dew-point temperature.

The electric heating/cooling microgrid does not contain CCHP unit, while the CCHP microgrid does not contain EHs/ECs, so the variables related to the CCHP unit and EHs/ECs in the objective function and constraint conditions should be removed respectively when establishing the optimization models for electric heating/cooling microgrid and CCHP microgrid.

5. Case Study

In order to verify the effectiveness of the proposed optimization model for r-microgrid scheduling, case studies are performed respectively for electric heating/cooling microgrid and CCHP microgrid which contain the residential building referred to in Section 2.2. The r-microgrids are optimized one day ahead with 1 h scheduling periods numbering 24 in total, and scenes of heating in winter and cooling in summer are considered, respectively.

5.1. Data of the Case

In the case studies, the parameters of the MTs, BESS, EHs, ECs, WT and PV are shown in Tables 6–10. The natural gas price $c_{gs} = 2.40$ CNY/m³, and the calorific value of natural gas $L_{HVNG} = 34.92$ MJ/m³. The lower limits of power purchasing/selling are $\underline{P}_{grid+} = \underline{P}_{grid-} = 0$ kW, and the upper limits of power purchasing/selling are $\overline{P}_{grid+} = \overline{P}_{grid-} = 600$ kW.

A typical day in summer as well as a typical day in winter in Hebei Province of China are selected to perform the scheduling process, of which the forecasted solar radiation intensity and outdoor temperature are shown in Figure 6, while the forecasted PV output, forecasted WT output, forecasted electric load and price for purchasing electricity from external grid are shown in Figure 7. The peak–valley price for purchasing electricity released by Hebei Southern Grid is used in this paper, and the price for selling electricity to external grid is set to be 80% of the price for purchasing electricity.

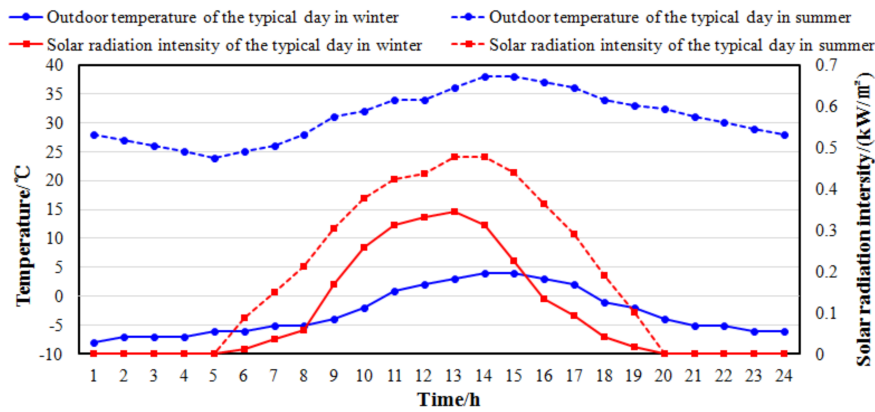


Figure 6. Forecasted solar radiation intensity and outdoor temperature.

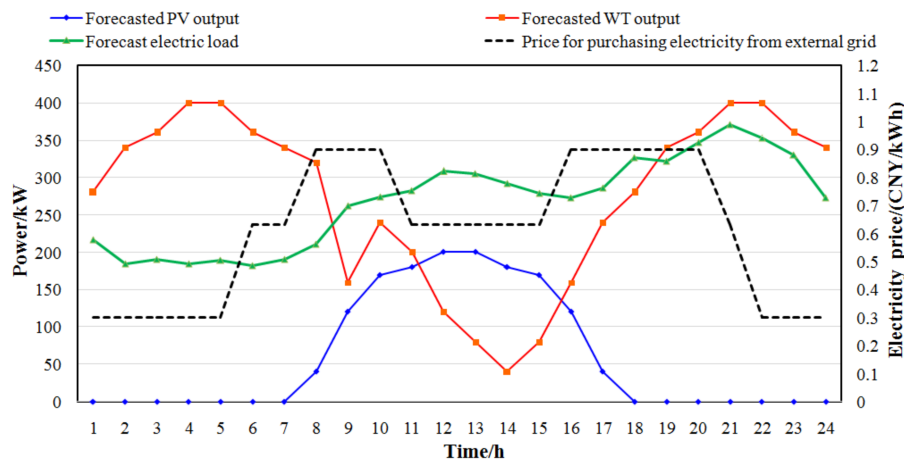


Figure 7. Forecasted PV output, WT output, electric load, and electricity price.

Table 6. Parameters of MTs [16].

Type	Number of Units	\overline{P}_{MT} (kW)	P_{MT} (kW)	c_{MT} (CNY/MWh)	η_L	η_{HE}
C200	3	600	60	30	0.01	0.9

Table 7. Parameters of BESSs [16].

η_c/η_{disc}	\overline{P}_{Si+} (kW)	\overline{P}_{Si-} (kW)	\overline{E} (kWh)	\underline{E} (kWh)	E^0 (kWh)	c_{Si+}/c_{Si-}
0.9	80	80	550	50	150	0.01

Table 8. Parameters of EHs.

Type	\overline{P}_{EH} (kW)	P_{EH} (kW)	COP_{EH}	c_{EH} (CNY/MWh)
CWDZ1080-85/70	1080	0	0.99	10

Table 9. Parameters of ECs [16].

\overline{P}_{EC} (kW)	P_{EC} (kW)	COP_{EC}	c_{EC} (CNY/MWh)
1000	0	4	10

Table 10. Parameters of WT and PV [16]

Type	Rated Power (kW)	Maintenance Cost (CNY/MWh)
WT	400	110
PV	300	80

Based on the above data, the presented MINLP optimization models for r-microgrids are solved by branch and bound method to get the optimal scheduling results. The solving process is implemented with LINGO11 software installed on a computer of which the master frequency of CPU is 1.7 GHz and memory is 4 GB.

5.2. Scheduling Results Analysis

In this paper, the optimal scheduling results of electric heating/cooling microgrid and CCHP microgrid with heavy floor VESSs are analyzed respectively, and comparisons are made between them and the optimal scheduling results with light floor VESSs.

5.2.1. Optimal Scheduling Results of Electric Heating/Cooling Microgrid

(1) Optimal scheduling results without heavy floor VESS

The operative temperature is kept at the optimum operative temperature (T_{zopt} is 22 °C for winter and is 25 °C for summer) when the electric heating/cooling Microgrid is optimized without VESS. The optimal scheduling results for typical day in winter as well as typical day in summer are shown respectively in Figure 8a,b, including the power exchange with external grid, the power consumed by EHs/ECs, the charging/discharging power of the BESS, the operative temperature and the radiant floor surface temperature. In order to facilitate the representation, the power selling to external grid and charging power of the BESS are taken negative in Figure 8. Meanwhile, in order to illustrate the pure effect of the VESS later, the corresponding optimal scheduling results of electric heating/cooling Microgrid without BESS are shown in Figure 9.

It is known that the charging/discharging behavior of the BESS is mainly influenced by electricity price, charging behavior usually happens at lower electricity price periods, while discharging behavior usually happens at higher electricity price periods. The power exchange with external grid and the power consumed by EHs/ECs in Figure 8 are quite similar with that in Figure 9. Power consumed by EHs/ECs is mainly determined by solar radiation intensity and outdoor temperature. Because both outdoor temperature and solar radiation intensity in the daytime are higher than that in the nighttime, for typical day in winter, the power consumed by EHs in the daytime is obviously lower than that in the nighttime; while for typical day in summer, the power consumed by ECs in the daytime is obviously higher than that in the nighttime. There is few electric power selling to the external grid for typical day in winter, while there is some electric power selling to the external grid for typical day in summer. The operating costs of the electric heating/cooling Microgrid for typical day in winter and typical day in summer are 4224.71 CNY and 596.93 CNY respectively, while without BESS, the corresponding operating costs are 4432.78 CNY and 786.08 CNY respectively.

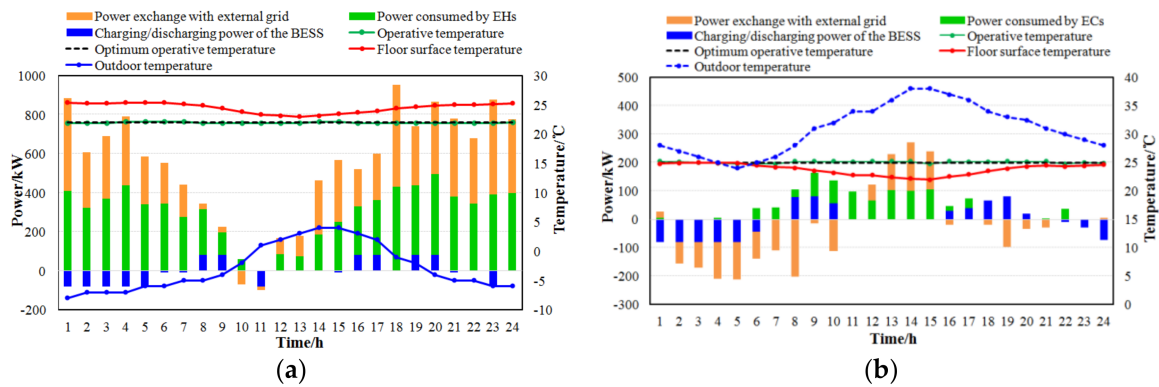


Figure 8. Optimal scheduling results of electric heating/cooling Microgrid without VESS. (a) Typical day in winter; (b) Typical day in summer.

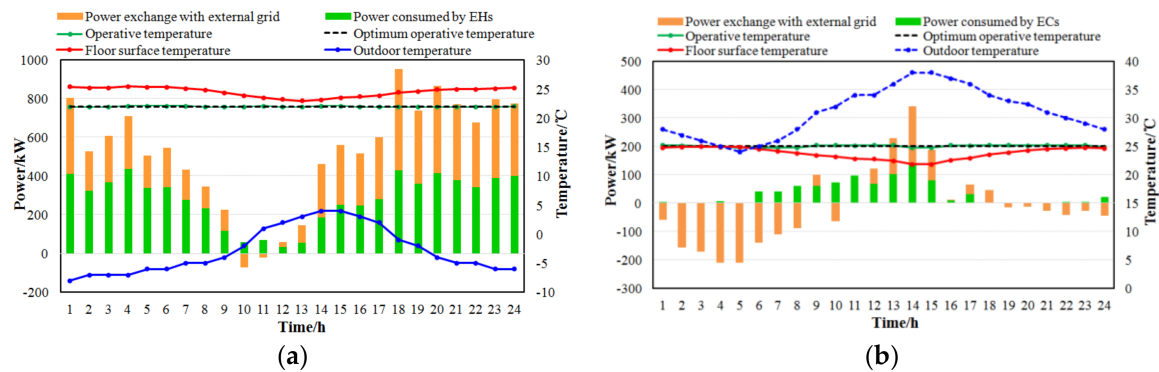


Figure 9. Optimal scheduling results of electric heating/cooling Microgrid without VESS and BESS. (a) Typical day in winter; (b) Typical day in summer.

(2) Optimal scheduling results with heavy floor VESSs

The operative temperature is kept around the optimum operative temperature (T_{zopt} is 22 °C for winter and is 25 °C for summer) with adjustable range of ± 2.5 °C when the electric heating/cooling microgrid is optimized with VESSs. The optimal scheduling results (thermal comfort sensitive coefficient $\gamma = 0.1$) for typical day in winter and typical day in summer are shown respectively in Figure 10a,b. Meanwhile, the corresponding optimal scheduling results of electric heating/cooling microgrid without BESSs are shown in Figure 11.

It is known that for BESS, charging behavior usually happens at lower electricity price periods, while discharging behavior usually happens at higher electricity price periods, which is quite similar with the scheduling results without VESSs. Power consumed by EHS/ECs and the operative temperature are quite different with the scheduling results without VESSs. At lower electricity price periods, more power is consumed by EHS/ECs, thus the operative temperature rises slowly on a typical day in winter while it falls slowly on a typical day in summer; at higher electricity price periods, less power is consumed by EHS/ECs, thus the operative temperature falls slowly in typical day in winter while rises slowly in typical day in summer. For a typical day in winter, it appears that some electric power is sold to the external grid at higher electricity price periods; for a typical day in summer, more electric power is sold to the external grid at higher electricity price periods. The operating costs of the electric heating/cooling microgrid with VESSs for a typical day in winter and typical day in summer are 3183.60 CNY and 388.16 CNY respectively, which decrease 24.64% and 34.97% respectively compared with the scheduling results without VESSs; while without BESSs,

the corresponding operating costs are 3334.83 CNY and 616.82 CNY respectively, which decrease 24.77% and 21.53% respectively compared with the scheduling results without VESSs.

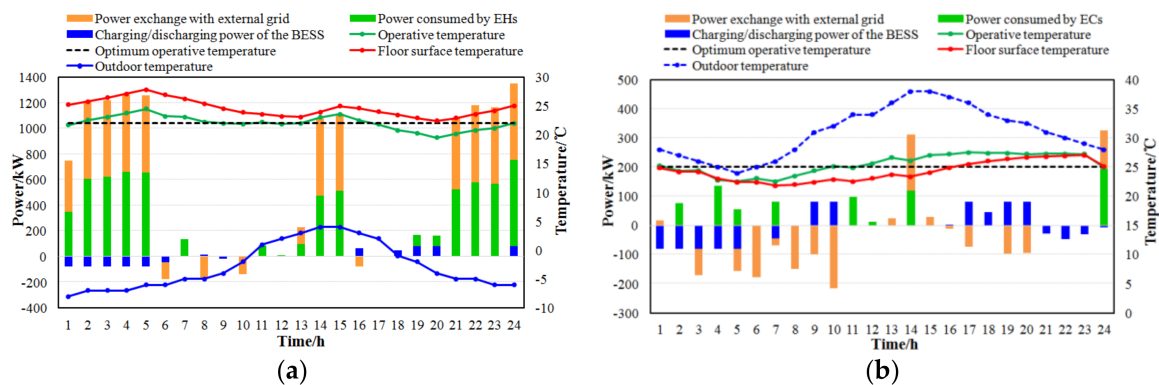


Figure 10. Optimal scheduling results of electric heating/cooling Microgrid with VESS and BESS. (a) Typical day in winter; (b) typical day in summer.

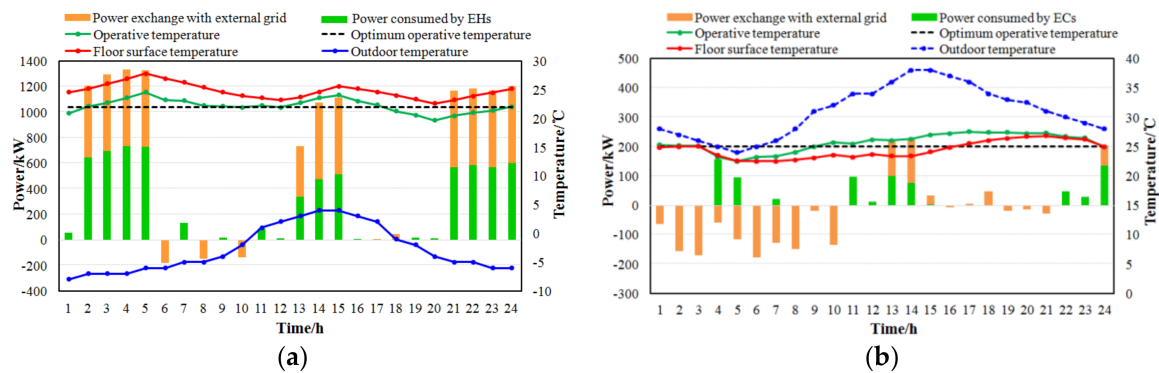


Figure 11. Optimal scheduling results of electric heating/cooling Microgrid with VESS and without BESS. (a) Typical day in winter; (b) typical day in summer.

(3) Charging/discharging characteristics of heavy floor VESSs

For electric heating/cooling microgrids, the power consumed by EHS/ECs is represented as the heating/cooling demand of residential buildings, then heating/cooling demand curves with/without VESSs are shown in Figure 12. Meanwhile, the corresponding heating/cooling demand curves of electric heating/cooling microgrids without BESSs are shown in Figure 13.

Take the heating/cooling demand curve without VESSs as reference curve, it could be understood that the heating/cooling demand curve with VESSs fluctuates around the reference curve. The part above the reference curve means heat/cool energy is stored in VESSs, which can be regarded as ‘charging’; while the part below the reference curve means heat/cool energy is released from the VESS, which can be regarded as ‘discharging’. The heating/cooling demand difference between the two cases is the charging/discharging power of a VESS. It is known that charging/discharging power of VESSs in Figure 12 are quite close to that in Figure 13, which indicates that BESSs have little impact on the charging/discharging characteristics of VESSs.

Comparing the charging/discharging power of VESSs in Figure 12 with the optimal scheduling results of BESSs in Figures 8 and 10, it can be seen that both VESSs and BESSs could enact reasonable charging/discharging responses to the variation of the electricity price. In addition, similar to the BESSs, the heavy floor VESSs could continuously work in ‘charging’ or ‘discharging’ states over multiple periods owing to the considerable thermal storage capacity of the radiant floor and envelope structure.

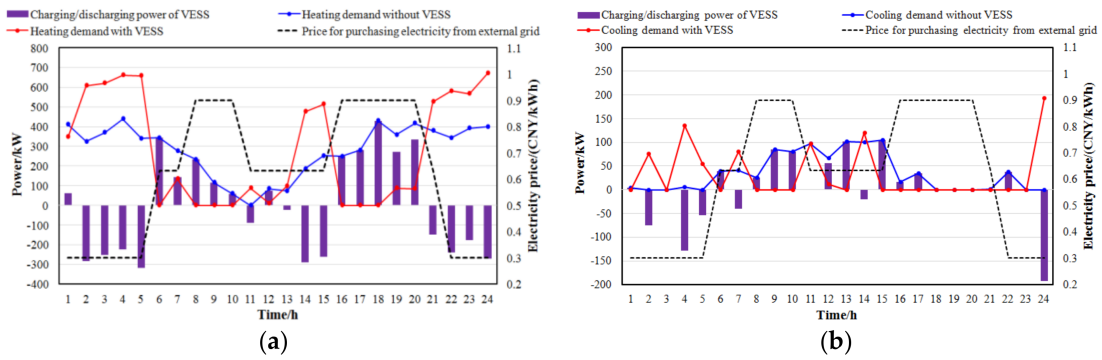


Figure 12. Charging/discharging power of VESSs for heating/cooling microgrids with BESSs. (a) Typical day in winter; (b) typical day in summer.

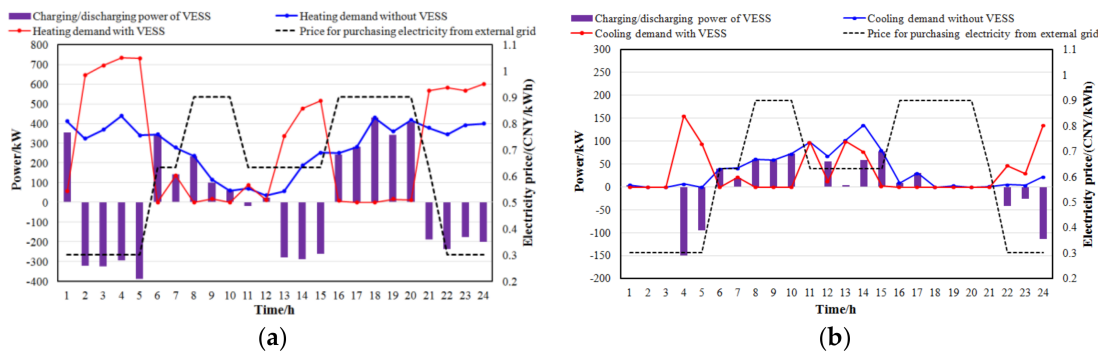


Figure 13. Charging/discharging power of VESSs for heating/cooling microgrids without BESSs. (a) Typical day in winter; (b) typical day in summer.

(4) Effect of thermal comfort sensitive coefficient on the scheduling results

Considering users’ different requirements for indoor thermal comfort level, take typical day in winter as example, the thermal comfort sensitive coefficient γ is adjusted, and the corresponding scheduling results of VESSs are shown in Figure 14. It can be found that the charging/discharging behaviors of the VESSs for different γ are basically consistent, that is, the charging process mainly happens at the lower electricity price periods, and the discharge process mainly happens at the higher electricity price periods. The larger the γ is, the less obvious the charging/discharging behavior of VESSs is due to the more serious punishment to the decline of thermal comfort level in the optimization model.

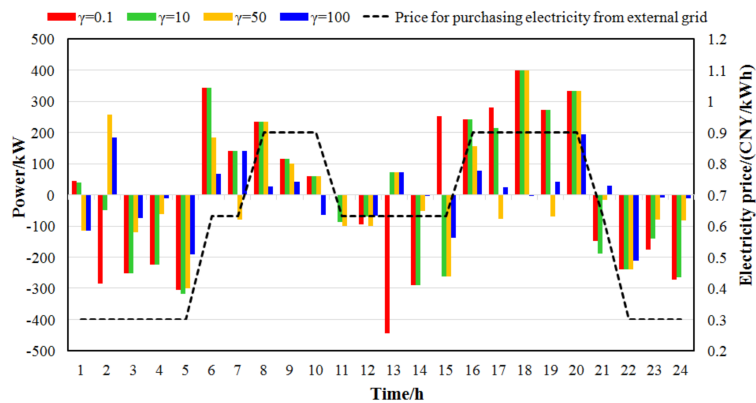


Figure 14. Scheduling results of charging/discharging behavior of VESSs for different γ .

The operative temperature curves for different γ are shown in Figure 15. It can be seen that the larger the γ is, the smaller the fluctuation of the operative temperature is due to the more serious punishment of the decline of thermal comfort level in the optimization model. The operating cost of the microgrid and average deviation of the operative temperature to the optimum operative temperature are calculated for different γ s, as shown in Table 11. It is known that the larger the γ is, the smaller the average deviation of the operative temperature is but the higher the operating cost of the microgrid is.

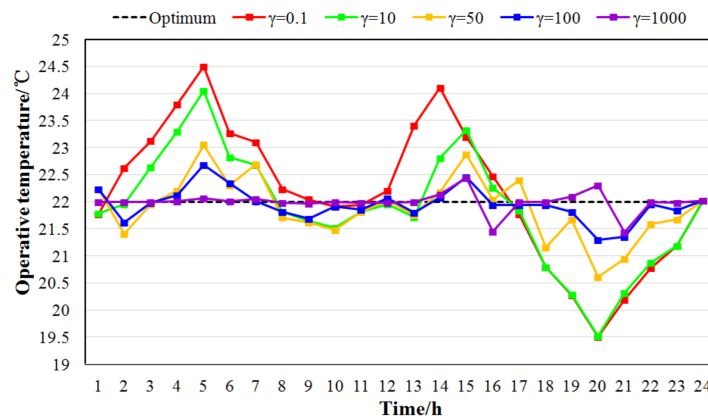


Figure 15. Curves of operative temperature for different γ s.

Table 11. Average deviation of operative temperature and operating cost of a microgrid for different γ s.

γ	0.1	10	50	100	1000
Daily operating cost of microgrid (CNY)	3183.60	3197.88	3623.51	3980.05	4205.31
Average deviation of operative temperature (°C)	1.00	0.79	0.44	0.22	0.10

5.2.2. Optimal Scheduling Results of CCHP Microgrids

(1) Optimal scheduling results without heavy floor VESSs

The operative temperature is also kept at the optimum operative temperature (T_{zopt} is 22 °C for winter and is 25 °C for summer) when the CCHP Microgrid is optimized without VESSs. The optimal scheduling results for a typical day in winter and a typical day in summer are shown respectively in Figure 16a,b, including the power exchange with external grid, the output electric power of MTs, the charging/discharging power of the BESSs, the operative temperature and the radiant floor surface temperature.

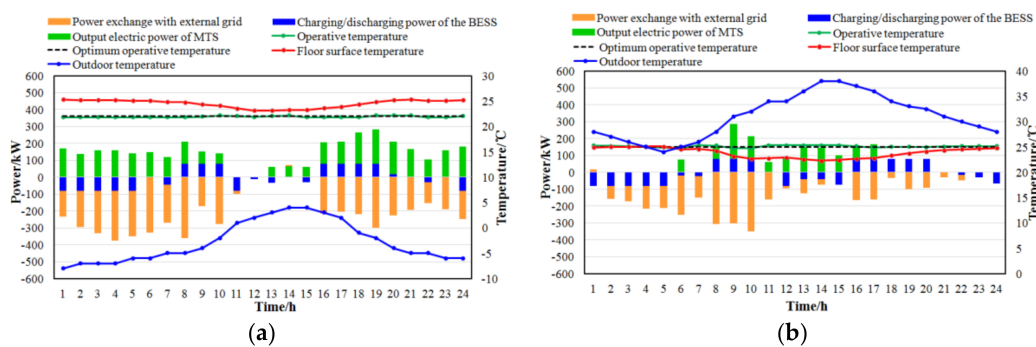


Figure 16. Optimal scheduling results of a CCHP microgrid without a VESS. (a) Typical day in winter; (b) typical day in summer.

It can be seen that the charging/discharging behaviors of BESS are mainly influenced by electricity price, which is quite similar to that of the electric heating/cooling microgrid. As the CCHP unit operates with the strategy of FTL, the output electric power of MTs depends on the heating/cooling demand determined by the outdoor temperature and the solar radiation intensity. For a typical day in winter, the output electric power of MTs in the daytime is obviously lower than that in the nighttime. While for typical day in summer, the output electric power of MTs in the daytime is obviously higher than that in the nighttime. There is almost no electric power purchasing from the external grid for both a typical day in winter and a typical day in summer. The operating costs of the CCHP microgrid for a typical day in winter and a typical day in summer are 1127.86 CNY and 303.27 CNY respectively.

(2) Optimal scheduling results with heavy floor VESSs

The operative temperature is also kept around the optimum operative temperature (T_{zopt} is 22 °C for winter and is 25 °C for summer) with adjustable range of ± 2.5 °C when the CCHP microgrid is optimized with a VESS. The optimal scheduling results (thermal comfort sensitive coefficient $\gamma = 1$) for a typical day in winter and a typical day in summer are shown respectively in Figure 17a,b.

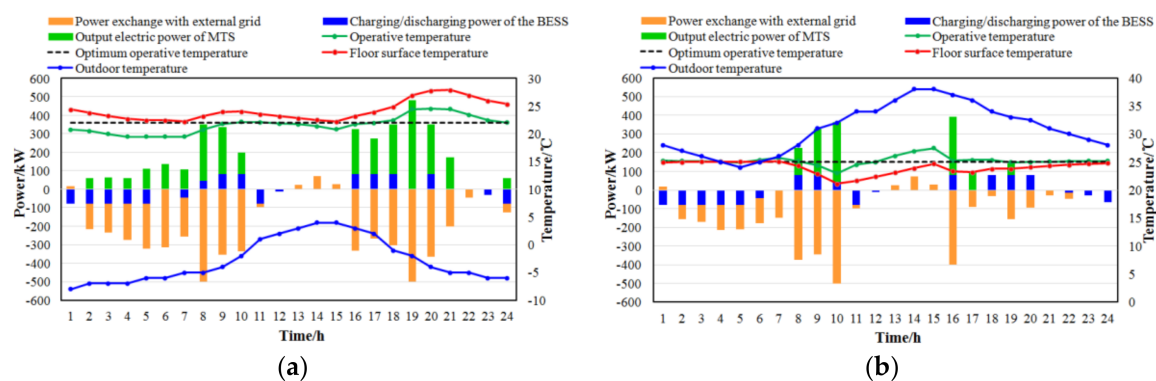


Figure 17. Optimal scheduling results of a CCHP microgrid with a VESS. (a) Typical day in winter; (b) typical day in summer.

It can be seen that the charging/discharging behaviors of BESSs are mainly influenced by electricity price, which is quite similar with the scheduling results without VESS. The output electric power of MTs is quite different with the scheduling results without VESS. At lower electricity price periods, less electric power as well as thermal power are generated by MTs, thus the operative temperature falls slowly on a typical day in winter while it rises slowly on a typical day in summer; at higher electricity price periods, more electric power as well as thermal power are generated by MTs, thus the operative temperature rises slowly on a typical day in winter while it falls slowly on a typical day in summer. For a typical day in winter and a typical day in summer, more electric power is sold to the external grid at higher electricity price periods. The operating costs of the CCHP microgrid for a typical day in winter and a typical day in summer are 657.01 CNY and 209.77 CNY respectively, which decrease 41.75% and 30.83% respectively compared with the scheduling results without VESSs.

(3) Charging/discharging characteristics of VESSs

For CCHP microgrids, the output thermal power of MTs could represent the heating/cooling demand of the residential building, then heating/cooling demand curves with/without VESSs are shown in Figure 18.

Take the heating/cooling demand curve without VESSs as a reference curve, it also could be understood that the heating/cooling demand curve with VESS fluctuates around the reference curve corresponding to the charging/discharging of the VESSs. Contrary to the VESSs in electric heating/cooling microgrids, the VESSs in CCHP microgrids work in a charging state at higher

electricity price periods while in a discharging state at lower electricity price periods. This is because the MTs need to generate more thermal power to increase the electric power sales to the grid at higher electricity price periods, which corresponds to the charging behavior of VESSs, and the MTs need to generate less thermal power to decrease the electric power selling to the grid at lower electricity price periods, which corresponds to the discharging behavior of VESSs.

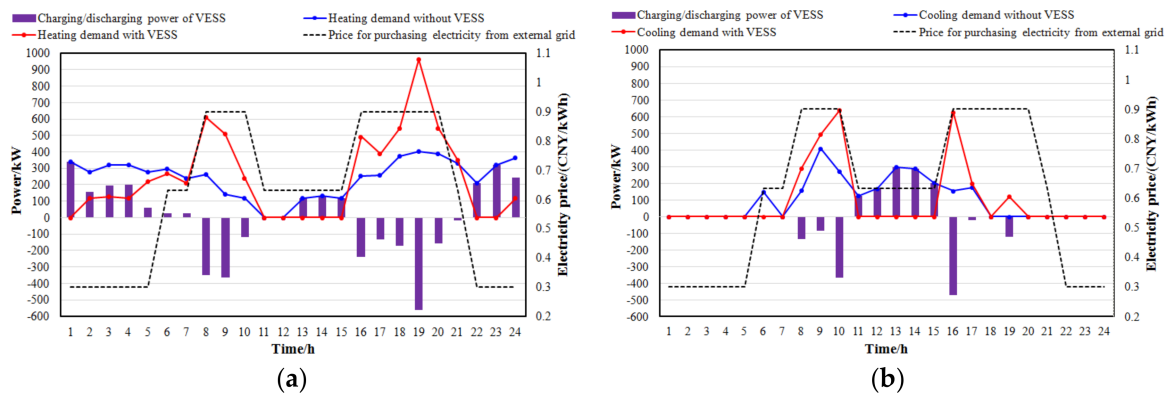


Figure 18. Charging/discharging power of VESSs for CCHP microgrids. (a) Typical day in winter; (b) typical day in summer.

5.2.3. Contrast of Scheduling Results for R-Microgrids with Light/ Heavy Floor VESSs

Take a typical day in winter as an example, the scheduling results of operative temperature and operating cost for r-microgrids with a light floor VESS and a heavy floor VESS are compared.

(1) Operative temperature contrast

For electric heating/cooling microgrids and CCHP microgrids with light floor VESSs, the corresponding scheduling result of operative temperature with different γ s are shown in Figure 19a,b respectively.

Compared with the operative temperature with heavy floor VESSs in Figure 15, it is known that the operative temperature with light floor VESSs fluctuates more frequently due to the relative weak thermal storage capacity of the light floor. In addition, when smaller γ is given in the optimization model, the operative temperature equals the lower limit for most scheduling periods, and only changes at the scheduling periods before or after the electricity price varies, which indicates that the continuity of the charging/discharging behavior of light floor VESS is relatively poor.

(2) Operating cost contrast

For electric heating/cooling Microgrid and CCHP Microgrid, the corresponding operating costs with heavy floor VESS and light floor VESS are shown respectively in Tables 12 and 13. It is known that, for all cases, the smaller the γ is, the lower the operating cost is. Compared with the scheduling result without VESS, for both electric heating/cooling microgrids and CCHP microgrids, more decrease of operating costs could be achieved with heavy floor VESSs than with light floor VESSs when a smaller γ is given in the optimization model. Take $\gamma = 0.1$ as an example, for electric heating/cooling microgrids, the operating cost can be decreased by 24.64% with heavy floor VESSs and only 10.37% with light floor VESSs; for the CCHP Microgrid, the operating cost can be decreased by 42.53% with heavy floor VESSs and only 8.87% with light floor VESSs.

Table 12. Operating cost of electric heating/cooling microgrids with different types of radiant floors (CNY).

γ	0.1	1	10	100	Without VESS
Light floor	3786.48	3807.77	4119.07	4223.18	4224.76
Heavy floor	3183.60	3197.88	3623.51	3980.05	4224.71

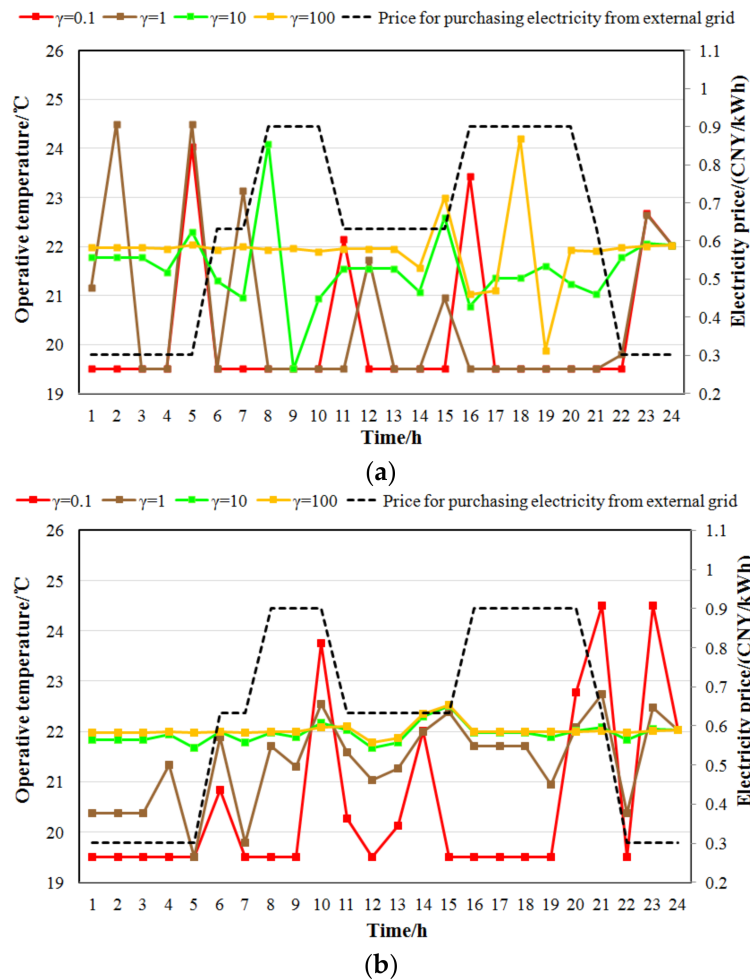


Figure 19. Curves of operative temperature for different γ s. (a) Electric heating/cooling microgrid; (b) CCHP microgrid.

Table 13. Operating cost of CCHP microgrids with different types of radiant floors (CNY).

γ	0.1	1	10	100	Without VESS
Light floor	1027.47	1070.27	1120.35	1126.46	1127.51
Heavy floor	648.19	657.01	860.26	1079.29	1127.86

6. Conclusions

In this paper, the radiant floor heating/cooling system is treated as a VESS for its considerable thermal storage capacity, and a novel R-Microgrid scheduling method with VESS is presented. The following conclusions are drawn:

- (1) For electric heating/cooling microgrids, the VESS works in charging state at lower electricity price periods while in discharging state at higher electricity price periods; for CCHP microgrids, on the contrary, the VESS works in charging state at higher electricity price periods while in discharging state at lower electricity price periods.
- (2) The thermal comfort sensitive coefficient γ has a marked influence on the scheduling result of the VESS. The larger the γ is, the less obvious the charging/discharging behavior of VESS is, and the smaller the average deviation of the operative temperature is while the higher the operating cost of the microgrid is.
- (3) Heavy floor VESSs could continuously work in charging state or discharging state over multiple scheduling periods, and the corresponding operative temperature fluctuates quite slowly.
- (4) For light floor VESSs, the continuity of the charging/discharging behavior is relatively poor, and the corresponding operative temperature fluctuates more frequently.
- (5) For both electric heating/cooling microgrids and CCHP microgrids, a greater decrease of operating costs could be achieved with heavy floor VESSs than with light floor VESSs.

Acknowledgments: The authors would like to acknowledge the financial support from the Beijing Natural Science Foundation (4182061) and the Fundamental Research Funds for the Central Universities (2017MS134, 2018ZD05).

Author Contributions: Weiliang Liu proposed the original idea and established the optimization model. Changliang Liu and Yongjun Lin checked the results of the whole manuscript. Liangyu Ma double-checked the results and helped to improve the full manuscript. Kang Bai and Yanqun Wu performed the main research tasks and translated the original manuscript.

Conflicts of Interest: The authors declare no conflict of interest.

References

1. Keirstead, J.; Jennings, M.; Sivakumar, A. A review of urban energy system models: Approaches, challenges and opportunities. *Renew. Sustain. Energy Rev.* **2012**, *16*, 3847–3866. [[CrossRef](#)]
2. International Energy Agency. *Energy Technology Perspectives 2012: Pathways to a Clean Energy System*; International Energy Agency: Paris, France, 2012.
3. Jin, X.; Wu, J.; Mu, Y.; Wang, M.; Xu, X.; Jia, H. Hierarchical microgrid energy management in an office building. *Appl. Energy* **2017**, *208*, 480–494. [[CrossRef](#)]
4. Yu, J.; Tian, L.; Xu, X.; Wang, J. Evaluation on energy and thermal performance for office building envelope in different climate zones of China. *Energy Build.* **2015**, *86*, 626–639. [[CrossRef](#)]
5. Guan, X.; Xu, Z.; Jia, Q. Energy-efficient buildings facilitated by microgrid. *IEEE Trans. Smart Grid* **2010**, *1*, 243–252. [[CrossRef](#)]
6. Xu, X.; Jia, H.; Wang, D.; Yu, D.C.; Chinag, H.D. Hierarchical energy management system for multi-source multi-product microgrids. *Renew. Energy* **2015**, *78*, 621–630. [[CrossRef](#)]
7. Jaramillo, L.B.; Weidlich, A. Optimal microgrid scheduling with peak load reduction involving an electrolyzer and flexible loads. *Appl. Energy* **2016**, *169*, 857–865. [[CrossRef](#)]
8. Lu, Y.; Wang, S.; Sun, Y.; Yan, C. Optimal scheduling of buildings with energy generation and thermal energy storage under dynamic electricity pricing using mixed-integer nonlinear programming. *Appl. Energy* **2015**, *147*, 49–58. [[CrossRef](#)]
9. Zhao, Y.; Lu, Y.; Yan, C.; Wang, S. MPC-based optimal scheduling of grid-connected low energy buildings with thermal energy storages. *Energy Build.* **2015**, *86*, 415–426. [[CrossRef](#)]
10. Li, Z.; Zhang, F.; Liang, J.; Yun, Z.; Zhang, J. Optimization on microgrid with combined heat and power system. *Proc. CSEE* **2015**, *35*, 3569–3576. (In Chinese)
11. Wu, X.; Wang, X.; Wang, J.; Bie, C. Economic generation scheduling of a microgrid using mixed integer programming. *Proc. CSEE* **2013**, *33*, 1–8. (In Chinese)
12. Lu, N. An evaluation of the HVAC load potential for providing load balancing service. *IEEE Trans. Smart Grid* **2012**, *3*, 1263–1270. [[CrossRef](#)]
13. Wang, C.; Liu, M.; Lu, N. A tie-line power smoothing method for microgrid using residential thermostatically-controlled loads. *Proc. CSEE* **2012**, *2*, 36–43. (In Chinese)

14. Ai, X.; Zhao, Y.; Zhou, S. Study on virtual energy storage features of air conditioning load direct load control. *Proc. CSEE* **2016**, *36*, 1596–1603. (In Chinese)
15. Jia, H.; Qi, Y.; Mu, Y. Frequency response of autonomous microgrid based on family-friendly controllable loads. *Sci. China Technol. Sci.* **2013**, *43*, 247–256. (In Chinese) [[CrossRef](#)]
16. Jin, X.; Mu, Y.; Jia, H. Optimal scheduling method for a combined cooling, heating and power building microgrid considering virtual storage system at demand side. *Proc. CSEE* **2017**, *37*, 581–590. (In Chinese)
17. Jin, X.; Mu, Y.; Jia, H.; Wu, J.; Tao, J.; Yu, X. Dynamic economic dispatch of a hybrid energy microgrid considering building based virtual energy storage system. *Appl. Energy* **2016**, *194*, 386–398. [[CrossRef](#)]
18. Van, R.J.; Leemput, N.; Geth, F.; Büscher, J.; Salenbien, R.; Driesen, J. Electric vehicle charging in an office building microgrid with distributed energy resources. *IEEE Trans. Sustain. Energy* **2014**, *5*, 1–8. [[CrossRef](#)]
19. Igualada, L.; Corchero, C.; Cruz-Zambrano, M.; Heredia, F.J. Optimal energy management for a residential microgrid including a vehicle-to-grid system. *IEEE Trans. Smart Grid* **2014**, *5*, 2163–2172. [[CrossRef](#)]
20. Rabiee, A.; Sadeghi, M.; Aghaei, J.; Heidari, A. Optimal operation of microgrids through simultaneous scheduling of electrical vehicles and responsive loads considering wind and PV units uncertainties. *Renew. Sustain. Energy Rev.* **2016**, *57*, 721–739. [[CrossRef](#)]
21. Lim, J.H.; Jo, J.H.; Kim, Y.Y.; Yeo, M.S.; Kim, K.W. Application of the control methods for radiant floor cooling system in residential buildings. *Build. Environ.* **2006**, *41*, 60–73. [[CrossRef](#)]
22. Zhao, K.; Liu, X.; Jiang, Yi. Dynamic performance of water-based radiant floors during start-up and high-intensity solar radiation. *Sol. Energy* **2014**, *101*, 232–244. [[CrossRef](#)]
23. Saponara, S.; Bacchillone, T. Network architecture, security issues, and hardware implementation of a home area network for smart grid. *J. Comput. Netw. Commun.* **2012**, *2012*, 534512. [[CrossRef](#)]
24. Saponara, S. Distributed Measuring System for Predictive Diagnosis of Uninterruptible Power Supplies in Safety-Critical Applications. *Energies* **2016**, *9*, 327. [[CrossRef](#)]
25. Wang, Z. *Low-Temperature Radiation Heating and Radiation Cooling*; China Machine Press: Beijing, China, 2004; pp. 120–127. (In Chinese)
26. Fanger, P.O. *Analysis and Applications in Environmental Engineering*; Thermal Comfort Analysis & Applications in Environmental Engineering; McGraw Hill: New York, NY, USA, 1970.



© 2018 by the authors. Licensee MDPI, Basel, Switzerland. This article is an open access article distributed under the terms and conditions of the Creative Commons Attribution (CC BY) license (<http://creativecommons.org/licenses/by/4.0/>).